Asymmetric hysteresis loops and smearing of the dielectric anomaly at the transition temperature due to space charges in ferroelectric thin films

I. B. Misirlioglu,[1,a)] M. B. Okatan,[2] and S. P. Alpay[2,3]
[1]*Faculty of Engineering and Natural Sciences, Sabancı University, Tuzla-Orhanli, 34956 Istanbul, Turkey*
[2]*Department of Chemical, Materials, and Biomolecular Engineering, Materials Science and Engineering Program, and Institute of Materials Science, University of Connecticut, Storrs, Connecticut 06269,USA*
[3]*Department of Physics, University of Connecticut, Storrs, Connecticut 06269, USA*

(Received 16 April 2010; accepted 29 May 2010; published online 5 August 2010)

Ferroelectric thin films often exhibit a displacement of the polarization versus the electric field hysteresis loops, particularly along the electric field axis. This shift is typically attributed to structural and electronic asymmetry of the film-electrode interfaces, asymmetric surface fields, as well as space charge regions. In this study, we analyze the effect of a spatial, continuous distribution of space charge on the hysteresis response and phase transition characteristics of epitaxial (001) $PbZr_{0.3}Ti_{0.7}O_3$ thin films sandwiched between metallic electrodes on (001) $SrTiO_3$ substrate. Using a nonlinear thermodynamic model, we compute numerically the internal electrical fields and polarizations for several different space charge distributions both in the presence of a triangular external electric field and as a function of temperature at zero applied field. We show that space charge accumulated near the metal-ferroelectric interfaces can dramatically displace the hysteresis along the electric field axis such that the otherwise symmetric coercive fields E_{C-} and E_{C+} in a bulk ferroelectric related to each other through $|E_{C-}|=E_{C+}$ may shift depending on the space charge concentration in such a manner that both $E_{C-},E_{C+}>0$ or $E_{C-},E_{C+}<0$. This gives rise to a very strong imprint. Our findings reveal that the presence of space charges in ferroelectric thin films results in significant changes in the phase transition characteristics, including a reduction in the phase transition temperature, smearing of the transition over a temperature range instead of a sharp dielectric anomaly at the bulk Curie temperature, and a reduction in the dielectric response compared to defect-free ferroelectrics of the same composition. © *2010 American Institute of Physics*. [doi:10.1063/1.3457348]

I. INTRODUCTION

All physical properties of ferroelectrics (FEs) are very sensitive to the presence of defects (vacancies, dislocations, impurities, etc.) and their concentration as these can alter the local dipole order due to the coupling of their eigenstrains and/or electrostatic fields with the polarization.[1–3] These materials are also wide band-gap semiconductors that produce Schottky-type interfaces when brought in contact with metallic electrodes.[4–8] Such effects become more pronounced in thin films and multilayers of FEs where imperfections such as oxygen vacancies inevitably form due to processing conditions[9,10] and linear defects such as misfit and threading dislocation may be generated because of the lattice misfit.[11] A number of studies have focused on the analysis of space charges in films and superlattices to distinguish the possible trapped charge contributions from real FE behavior of the samples.[11–14] The combination of the extrinsic factors such as trapped charges, concentration variations, and defects with local strain fields could reduce the polarization stability and the dielectric response.[2,3,15,16]

An important degradation mechanisms often observed in FEs is imprint. The most common characteristic of imprint is the displacement of the polarization versus the applied electric field hysteresis loop along the electric field axis. This gives rise to an asymmetry in the remnant polarization and also an effective variation in the coercive field defined by an off-set, $\Delta E=E_{C+}-E_{C-}$, where E_{C+} and E_{C-} are the coercive fields on the right and left side of the hysteresis loop, respectively. Imprint could result from elevated temperatures due to asymmetric migration of species along the film, exposure to UV light or x-rays[17] as well as asymmetric film-electrode top and bottom interfaces.[18] While the exact mechanisms of imprint are not known, there is strong experimental evidence that it results from trapped charges, charged defects, and other possible defect dipole complexes, surface fields, and stress gradients.

Deposition conditions of thin film materials are often far from ideal and hence kinetic factors play an important role in the ultimate stoichiometry of the film.[18–21] As perovskite FEs have a mix of ionic and covalent interatomic bonding, local deviations from the exact stoichiometry can create frozen dipoles and electrostatic fields emanating from these complexes. Furthermore, it has often been discussed that these "defects" can then trap carriers and become *p*- or *n*-type centers.[5–8,22] For instance, the surfaces of FE thin films are highly susceptible to creation of oxygen vacancies during processing and an electrode-FE film interface is often thought to be forming a Schottky contact and a commensurate depletion layer. While the effect of the internal electric

[a)]Electronic mail: birc@sabanciuniv.edu.

fields due to surfaces, structural variations, and trapped charges, and other defect microstructures on the properties of FEs is well-understood, theoretical studies of the imprint phenomenon have focused on charge injection and frozen average electrostatic fields.[3,6,7,10,23–30]

In a recent study, we have shown that internal voltage off-sets and imprint can result from asymmetrically distributed trapped space charges described through a constant planar space charge density in a simple FE capacitor structure using a nonlinear thermodynamic analysis coupled with electrostatics.[31] The electrostatic interactions are established through the built-in polarization due to the space charges and the spontaneous polarization. Although this simple approach wherein a monolithic FE is assumed to be composed of "sections" (or "layers") with different polarization values when a constant space charge is discretely inserted at a given position within the FE is able to explain the displacement of the FE hysteresis loops, it can be improved significantly if the limitations on the position and density of the space charges are removed. This is the topic of the current work in which we analyze FE films sandwiched between metallic electrodes and introduce position-dependent, continuous distribution of space charge along the thickness of the film. These charges are thought as fixed-field defects and are distributed inside the film as a function of position. Our findings reveal that the hysteresis characteristics of FE films can be altered dramatically under asymmetric spatial variations in the space charge density. For example, space charges asymmetrically accumulated near the electrode-film interfaces as low as $0.075\ \mathrm{C/m^2}$ can shift the entire hysteresis loop such that $E_{C^-}, E_{C^+} > 0$ or $E_{C^-}, E_{C^+} < 0$ compared to an "ideal" FE with $|E_{C^-}| = E_{C^+}$ and $\Delta E = E_{C^+} - |E_{C^-}| = 0$. It is also shown that space charges in FE thin films result in variation in the FE-paraelectric phase transition (PT) behavior, resulting in a reduction in the transition temperature and a smearing of the transition over a temperature range instead of the sharp dielectric anomaly at the bulk Curie temperature compared to defect-free "ideal" FEs of the same composition.

II. THEORY AND METHODOLOGY

Before we proceed with the thermodynamics of a FE film with an arbitrary volumetric variation in space charges, we first focus on the distribution of these in vacuum between two planar electrodes and their potential. We form a one-dimensional system where there could either be a discrete or a continuous distribution of charges. The system analyzed here has its boundaries along the z-axis and is infinite along other directions. A simple sandwich-type capacitor structure with a sheet charge situated at a point k will have an internal potential at a point j given by

$$\phi_{j,k} = \frac{\rho A z_j}{\varepsilon_0}\frac{(L - z_k)}{L} \quad \text{for } 0 \le z_j < z_k, \tag{1}$$

$$\phi_{j,k} = \frac{\rho A z_k}{\varepsilon_0}\frac{(L - z_j)}{L} \quad \text{for } z_k < z_j \le L, \tag{2}$$

which correspond to the analytical solutions of the Poisson's equation at all other points other than the charge location when the electrodes are kept at zero potential. In Eqs. (1) and (2), ρ is the charge density, A is the area of the capacitor, L is the distance between the electrodes, and ε_0 is the permittivity of free space. The indices serve to distinguish the position of the sheet charge and its potential at a given location such that $\phi_{j,k}$ stands for the potential at j due to a charge density situated at a point k. For example, it is clear that there will be two different fields in $+z$ and $-z$ whose magnitudes are equal (but of opposite sign) when the sheet charge is in the middle of the capacitor. We note that in the presence of a material between the electrodes, ε_0 should be replaced with $\varepsilon_r \cdot \varepsilon_0$ where ε_r is the background dielectric constant that is basically a measure of electronic polarizability of the ions. For a sheet of charge ρ fixed in the center, the fields pointing along $+z$ and $-z$ will be $\pm\rho/2\varepsilon_0$ when there is no material and $\pm\rho/2\varepsilon_0\varepsilon_r$ in the presence of a dielectric. Thus, in the presence of a dielectric, ε_0 should be replaced with $\varepsilon_r\varepsilon_0$. For this study, ε_r is taken as ten, corresponding to an optical frequency refractive index of ~ 3.16.[32]

In a periodic or random distribution of space charge, there can be a bias field along either $+z$ or $-z$ directions depending on the charge density as a function of position. We assign each discrete point k a planar charge density that is infinite along x- and y-axes, i.e., in the plane of the film-substrate interface. Hereafter, we approximate the total potential at each point inside the capacitor as a sum of all potentials due to all charges in the system at that point (excluding the particular point itself). Using this superposition principle of electrostatic potential due to a charge distribution in the space between two electrodes, we can discretewise approximate the total potential, ϕ at a point j due to the space charges situated at all k in our system as

$$\phi_j = \sum_k \phi_{j,k}. \tag{3}$$

Thus, ϕ_j defines the total potential at a point j due to all charges at points k. We consider four cases corresponding to the following distributions:

(i) exponentially but asymmetrically decaying charge density to zero from interfaces 1 (bottom electrode-FE) and 2 (FE-top electrode) toward the interior of the film [Fig. 1(a)] along with the induced built-in fields due to these distributions given in Fig. 1(b),
(ii) symmetrical charge at both interfaces decaying to zero in the middle of the film [Fig. 1(c)] with the corresponding built-in field in Fig. 1(c),
(iii) random distribution of space charge throughout the entire film, and,
(iv) no space charge as the reference state.

The first and second distributions are chosen to simulate interfaces that either have high concentration of traps at the FE-electrode interfaces or are due to a Schottky-behavior resulting from band bending. The third case corresponds to film with high density of charge trapping defects throughout the volume. The total number of discrete points in the system is 500 and each cell length is taken as 0.4 nm, close to the unit cell parameter of prototypical perovskite FEs such as barium titanate [$BaTiO_3$(BT)] or lead zirconate titanate

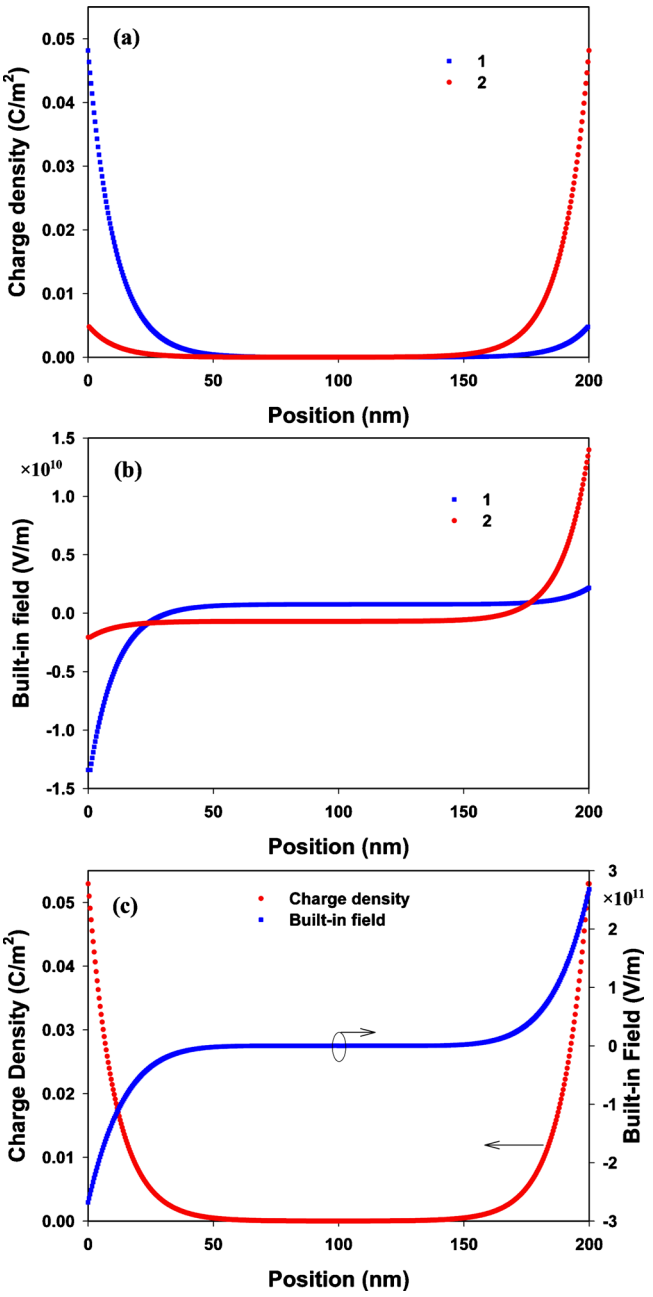

FIG. 1. (Color online) (a) The space charge distribution for the case of asymmetric exponential decay from both film-electrode interfaces toward the interior of the film. d1 and d2 correspond to exponential charge injection from the top and bottom electrodes, respectively; (b) the built-in field due to charge distributions d1 and d2 in (a); (c) a symmetric distribution of space charges and the corresponding built-in field.

$[PbZr_{1-x}Ti_xO_3(PZT\ x/1-x)]$ with Ti-rich stoichiometries. Once the total built-in potential at each point in the system is established, the local internal field E can simply be computed from the gradient of the potential ϕ_j along the z-axis via

$$E_j = -\nabla\phi_j. \tag{4}$$

We should also mention here that the above approach is for a capacitor whose electrodes are kept at zero potential. In the presence of an externally applied potential, where experimentally one electrode often attains a particular sign while the other is kept at ground, the internal total potential due to the space charge distribution might vary as the boundary conditions change for the solution of the Poisson's equation. Throughout the current work, we consider that the interaction of the applied potential with the space charge is via a straightforward vectorial addition of the electric fields at each point.

We now proceed with the thermodynamics of the FE film sandwiched between two electrodes and how space charge is introduced to the system energy. The Landau–Ginzburg–Devonshire free energy for an epitaxial monodomain (001) FE film on a (001) cubic substrate can be expressed as

$$F_T = \int_0^L [F_0 + F_P + F_E + F_G - F_{ES}]dz, \tag{5}$$

where L is the film thickness, F_0 is the energy of the paraelectric state,

$$F_P = \alpha_1(P_1^2 + P_2^2 + P_3^2) + \alpha_{11}(P_1^4 + P_2^4 + P_3^4) + \alpha_{12}(P_1^2P_2^2 + P_1^2P_3^2 + P_2^2P_3^2) + \alpha_{111}(P_1^6 + P_2^6 + P_3^6) + \alpha_{112}[P_1^4(P_2^2 + P_3^2) + P_2^4(P_1^2 + P_3^2) + P_z^4(P_1^2 + P_2^2)] + \alpha_{123}P_1^2P_2^2P_3^2, \tag{6}$$

is the energy due to the polarization P_i $(i=1,2,3)$ in the FE state, and α_i, α_{ij}, and α_{ijk} are the dielectric stiffness coefficients.[33] F_E in Eq. (5) is the internal elastic energy due to epitaxy given by

$$F_E = \frac{1}{S_{11}+S_{12}}(u_m - Q_{12}P_3^2)^2, \tag{7}$$

where u_m is the in-plane polarization-free misfit strain, $Q_{12}P_3^2$ is the self-strain in the plane of the film due to polarization along the film thickness, and Q_{ij} and S_{ij} are the electrostrictive coefficients and the elastic compliances at constant polarization, respectively, in the contracted notation.

The gradient energy in Eq. (5) is given by

$$F_G = G_{33}\left(\frac{dP_3}{dz}\right)^2 + G_{13}\left(\frac{dP_1}{dz}\right)^2 + G_{23}\left(\frac{dP_2}{dz}\right)^2, \tag{8}$$

where G_{ij} are the gradient energy coefficients.

The last term entering Eq. (5) is the electrostatic energy. In its most general form, it can be expressed as

$$F_{ES} = \left[E_{APP} + E(z) - \frac{1}{2}E_D(z)\right]P_3, \tag{9}$$

and the total field E_3 at a position j due to the electrostatic interactions is given as

$$E_3 = E_{APP} + E(z) - E_D(z). \tag{10}$$

In Eqs. (9) and (10), E_{APP} is the external applied field, $E(z)$ is the built-in field due to the space charges attaining its value from Eq. (4), and E_D is the depolarization field arising due to the polarization variations at the interfaces resulting in bound charges. $E(z)$ and E_D are both functions of position and the latter is given as

$$E_D(z) = \frac{1}{\varepsilon_r\varepsilon_0}\left[P_3 - \frac{1}{L}\int_0^L P_3 dz\right]. \tag{11}$$

For thin layers (at the order of a few nanometers) and highly inhomogeneous structures, the gradient energy may have a significant effect on polarization and cannot be neglected. In our calculations, we shall assume that the gradient energy is isotropic, and thus $G_{33}=G_{13}=G_{23}=G$. Furthermore, the in-plane biaxial internal stress state with equal orthogonal components due to epitaxy require that $P_1=P_2$. Thus we obtain the following Euler–Lagrange relations from the equations of state $\partial F_T/\partial P_3=0$ and $\partial F_T/\partial P_1=0$

$$G\frac{d^2P_3}{dz^2}=2\alpha_3^mP_3+4\alpha_{13}^mP_3P_1^2+4\alpha_{33}^mP_3^3+6\alpha_{111}P_3^5+\alpha_{112}(4P_3P_1^4+8P_3^3P_1^2)+2\alpha_{123}P_3P_1^4-\left[E_{APP}+E_B-\frac{1}{\varepsilon_r\varepsilon_0L}\int_0^L P_3dz\right], \tag{12}$$

$$G\frac{d^2P_1}{dz^2}=2\alpha_1^mP_1+2(2\alpha_{11}^m+\alpha_{12}^m)P_1^3+2\alpha_{13}^mP_1P_3^2+6\alpha_{111}P_1^5+2\alpha_{112}[3P_1^5+3P_1^3P_3^2+P_1P_3^4]+2\alpha_{123}P_1^3P_3^2, \tag{13}$$

where the α_3^m, α_{13}^m, and α_{33}^m are the renormalized dielectric stiffness coefficients, modified by the misfit strain, the depolarizing field, and the two-dimensional clamping of the film.[34] We note that the only dielectric stiffness coefficient that is renormalized due to the depolarizing field is α_3^m and is given by

$$\alpha_3^m=\alpha_1-u_m\frac{2Q_{12}}{S_{11}+S_{12}}+\frac{1}{\varepsilon_r\varepsilon_0}, \tag{14}$$

as a result of the emergence of the P_3^2/ε_0 term coming from the depolarization field energy [Eqs. (9)–(11)]. The boundary conditions at the interfaces employed for the films are

$$\left[P_1+\lambda\frac{dP_1}{dz}\right]_{z=0,L}=0, \tag{15a}$$

$$\left[P_3+\lambda\frac{dP_3}{dz}\right]_{z=0,L}=0, \tag{15b}$$

and λ is the extrapolation length. Equation (15b) implies that there are no surface fields at the FE-electrode interfaces. Therefore, the only depolarizing field contribution in the system are due to the local variations in P_3 induced by space charges, which are weakly screened by the background dielectric constant. The materials system considered in this study is a 200 nm thick heteroepitaxial (001) PZT 30/70 on a (001) $SrTiO_3$ (ST) substrate with pseudomorphic top and bottom metallic electrodes. The values of the dielectric stiffness coefficients and other thermodynamic parameters entering the calculations are given in Table I. The equations of state given in Eqs. (12) and (13) have to be solved simultaneously with the boundary conditions given in Eqs. (15a) and (15b). To obtain the polarizations at different space charge and applied fields and different temperatures, we use a Gauss–Seidel iterative scheme where we start with random polarization distributions in the system that converges to the real solution after a number of iterations.

TABLE I. Thermodynamic parameters, free energy coefficients, electromechanical, and elastic coefficients of PZT 30/70 used in this study, from Ref. 33.

	PZT 30/70
T_C (°C, bulk)	440
ε_0 (10^{-12} F/m)	8.85
C (°C)	1.5×10^5
α_{11} (10^7 m^5/C^2F)	0.6458
α_{111} (10^8 m^9/C^4F)	2.348
α_{12} (10^8 m^5/C^2F)	5.109
α_{112} (10^8 m^9/C^4F)	10.25
α_{123} (10^8 m^9/C^4F)	−5.003
S_{11} (10^{-12} Pa^{-1})	8.4
S_{12} (10^{-12} Pa^{-1})	−1.7
S_{44} (10^{-12} Pa^{-1})	9.24
Q_{11} (10^{-2} m^4/C^2)	7.887
Q_{12} (10^{-2} m^4/C^2)	−2.480
Q_{44} (10^{-2} m^4/C^2)	6.356
D_{33}, D_{13}, D_{23} (10^{-9} m^3/F)	5.0
λ (m)	Infinite
u_m at RT	−0.0166

The temperature-polarization ($T-P_3$) curves reflect the equilibrium polarization at each temperature interval in the presence and absence of space charge distribution. The quasistatic P_3-E_{APP} hysteresis curves are at room temperature (RT=25 °C) obtained by applying a triangular field that has a maximum amplitude of 5×10^8 V/m and incremental values of 2.5×10^7 V/m, adding up to a total of 100 steps. At each field, the polarization as a function of position is computed using the iterative method detailed above. In both the temperature dependence of the polarization and the hysteresis loop computations, the values of polarization obtained for a given state are fed as initial values for the next iterative run, ensuring high convergence precision. The small signal average dielectric constant of the system along z is found from

$$\varepsilon(T,\rho)=\frac{D_3(T,\rho,E_S)-D_3(T,\rho,E_{APP}=0)}{E_S}, \tag{16}$$

where D_3 is the dielectric displacement of the film along the z-axis obtained at the end of the numerical iteration for zero field followed by for a small signal field, $E_S=1$ V/m. The in-plane misfit strain considered in all computations corresponds to a pseudomorphic (001) PZT 30/70 film on a (001) ST substrate (−1.66% at room temperature). During the numerical iteration, although we took into account the possible presence of an in-plane polarization in PZT 30/70, the solution of the in-plane components comes out as zero for the considered strain state. In the $T-P$ plots, to be able clearly judge the effect of space charge and avoid complications due to thermal strain effects on the PT characteristics, we assumed both the substrate and the FE film have the same thermal expansion coefficients. The reason for this assumption is that while thermal strains as well as stress relaxation due to the formation of interfacial dislocations can easily be

incorporated into the current analysis, these might mask space charge related changes in the polarization and dielectric response.

III. RESULTS AND DISCUSSION

A. FE Hysteresis Loops

As one of the prominent observations in FE thin films compared to their bulk counterparts is the asymmetry in the $P-E_{APP}$ ($P=P_3$) hysteresis loops, we first focus on the effect of charge distributions at interfaces that decay exponentially toward the interior of the film. Such an accumulated charge density near interfaces will induce asymmetric potentials in the film resulting in internal electric fields that might favor an asymmetric variation in $P(z)$. An example of the charge distribution at interface 1 with a maximum planar density amplitude of 0.05 C/m^2 at interface 1 and 1/10th of this value at interface 2 (denoted as distribution 1 or d1), and vice versa (distribution 2, d2) are given in Fig. 1(a). The built-in fields associated with d1 and d2 are plotted in Fig. 1(b). The gradient of the potential is steeper toward interfaces, creating the highest internal fields in this region for both of the two cases. The maximum amplitude of the charge density can be adjusted or a random distribution could also be defined. We did so for maximum asymmetric local density amplitudes of 0.05 and 0.075 C/m^2 for both d1 and d2. Such a spatial density of space charge accumulating on either side of the capacitor structure should be expected to pin the polarization when the bias field it creates is comparable to the thermodynamic coercive field.

Assuming perfect electrodes and infinite extrapolation length at the interfaces, together with incorporation of the small screening contribution from the background dielectric constant to the depolarizing field term, we find the spontaneous polarization at zero field and RT the same as the analytically computed value (~ 0.7 C/m^2, $T_C \sim 900$ °C) for a monodomain pseudomorphic (001) PZT 30/70 film on (001) ST. We note that for a perfect film with perfect electrodes and infinite extrapolation length, there is no depolarization as the polarization is homogeneous throughout the thickness of the film. The $P-E$ hysteresis are computed for the charge density distributions given in Fig. 1 with the form of d1 and d2 for maximum planar densities of 0.05 C/m^2 and 0.075 C/m^2 displayed in Figs. 2(a) and 2(b), respectively. Changing the maximum local planar density amplitude to 0.075 C/m^2 does not change the form of the distribution but only the local values that are used to plot Fig. 1(b). As shown in Fig. 2, the shift of the hysteresis loops depends on the way space charge is distributed as well as its local concentration in the film. We note that we only exchange the amplitudes of planar space charges to obtain d1 and d2 but not the sign of charge. Furthermore, another important finding is that the $P-E_{APP}$ loops under asymmetrically distributed high space charge densities near the interfaces (such as in the case of 0.075 C/m^2 local planar density) can be shifted along the applied field axis such that $E_{C^-}, E_{C^+} > 0$ or $E_{C^-}, E_{C^+} < 0$ compared to charge-free films for which $|E_{C^-}| = E_{C^+}$ and $\Delta E = E_{C^+} - |E_{C^-}| = 0$ [also shown in Figs. 2(a)–2(c) as a reference]. Similar behavior was discussed in Ref. 2 where irradiated triglycine sulfate samples were shown to display strongly shifted or deformed hysteresis response. One must note here that a fixed space charge density is considered in this study within the thermodynamic limit. Changes in temperature and band bending during polarization switching of the electrode-FE-electrode system could make the space charge density a dynamic parameter where it becomes a function of the applied field.

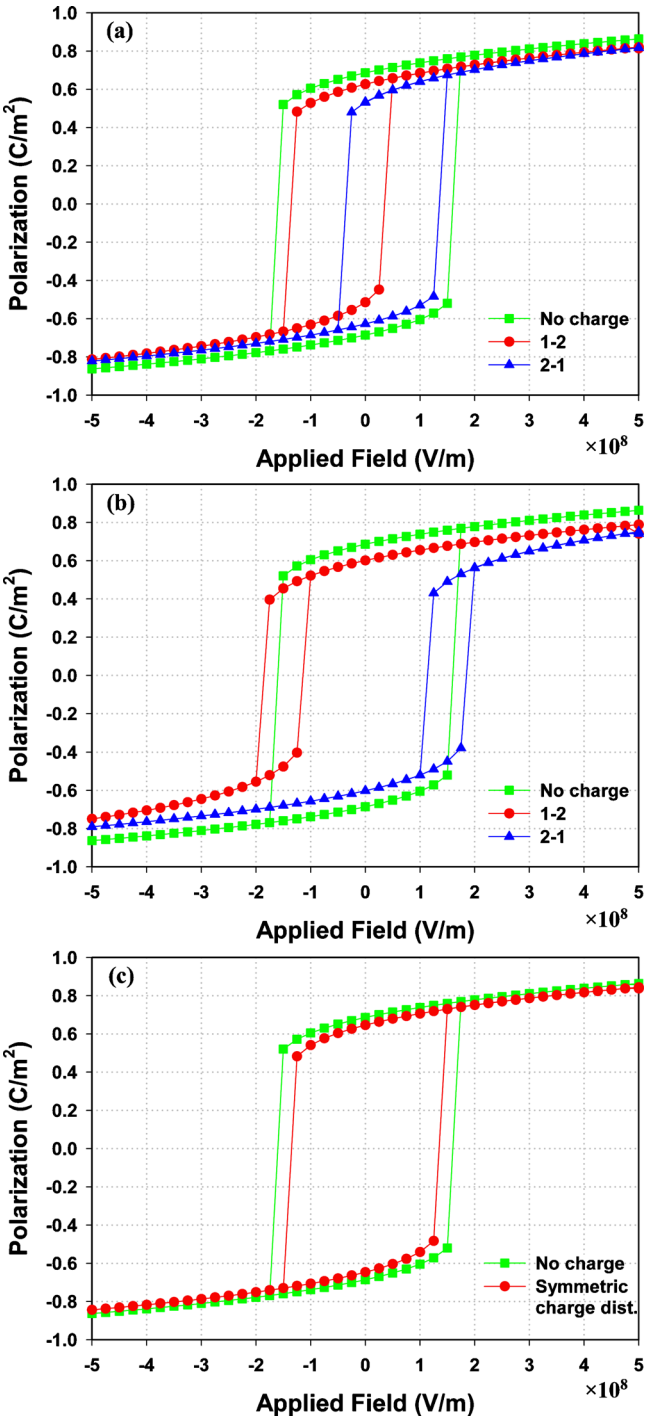

FIG. 2. (Color online) The displacement of the polarization-applied electric field hysteresis curves due to asymmetrically exponential decay of space charge distributions with a maximum amplitude of (a) 0.05 C/m^2 and (b) 0.075 C/m^2 with charge distribution d1 and d2, respectively; and (c) fully symmetric charge distribution with 0.05 C/m^2 at each interface. The hysteresis curves outlined by solid squares in (a), (b), and (c) correspond to films with no space charges.

To elucidate the formation of space charges even in nearly defect-free films where behavior similar to that in Fig. 2 might be observed, we provide the following example. Epitaxial growth of FE films on metallized single-crystal substrates is usually carried out at relatively high temperatures (typically in the range of 500–800 °C) in controlled oxygen atmospheres followed by cooling. The sample is then taken out of the chamber for the placement of a mask to enable the growth of top electrodes, typically achieved via rf-sputtering or thermal evaporation. The diameter of the top electrodes may vary from a few hundred nanometers to a few tens of microns. This processing sequence may actually promote an asymmetric charge injection at the two FE-electrode interfaces just because a different deposition method at a different temperature was used to grow the bottom electrode, the FE film, and the top electrode. Moreover, the formation of asymmetrical space charges may result from the termination of different atomic planes of the FE film. One must also note that an average negative bias due to asymmetric surface effects or near-interface charges displaces the hysteresis loop toward the positive E_{APP}-axis and vice versa.

In order to provide a complimentary view of the effect of distribution of the space charges throughout the film, we give in Fig. 2(c) the hysteresis loop of a FE film when there are equal concentrations of fixed space charges that decay exponentially from both interfaces. Due to the symmetry of the internal electric field distribution in the film, there is no displacement of the hysteresis loops but there is a considerable reduction in the coercive field, consistent with our recent findings.[17] This is due to the depolarization field that arises from the inhomogeneous variation in the polarization along the film thickness as well as the commensurate gradient energy. As such, the phase transition temperature T_C is reduced. The behavior of the total polarization as a function of the temperature is discussed in Sec. III B.

B. Phase transition temperature and dielectric properties

Using the methodology described in Sec. III A, we calculated the total polarization and the dielectric response of the FE film as a function of the temperature for a perfect film with no space charges and a film with asymmetric distribution of space charge densities. Figure 3 plots the temperature dependence of the polarization and the dielectric constant of the (001) PZT 30/70 film on (001) ST with no space charges and a space charge distribution d1 with a maximum amplitude of 0.05 C/m^2. For the case for $\rho=0$, the spontaneous polarization in the film vanishes above T_C, and, as expected, there is a λ-type anomaly in the dielectric response at T_C. However, if there is an inhomogeneous distribution of the space charges, the phase transformation is "smeared" over a temperature interval rather than a singular transition point as it is the case for $\rho=0$. Furthermore, there is also a significant reduction in the dielectric properties near T_C for films with asymmetric space charge distributions (Fig. 3). For asymmetric variations in the space charge, there is a nearly temperature-insensitive polarization above the effective T_C that is essentially the built-in polarization due to the space charges. For higher values of the space charge density, the

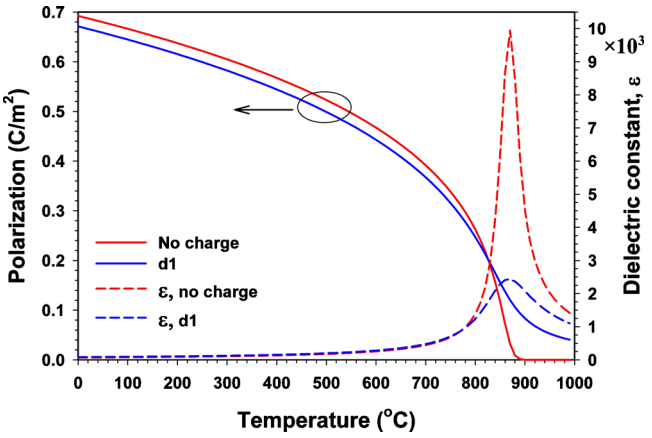

FIG. 3. (Color online) Total polarization and the dielectric constant as a function of temperature in the absence of space charges and with space charges (d1, with a maximum of 0.05 C/m^2).

transition becomes a very gradual one, almost a linear variation in polarization with temperature with no apparent phase transformation temperature. While there is a small reduction in the polarization values and T_C, the latter is considerably more pronounced for a system with a random distribution of space charges which will be discussed next. We note here the space charge concentrations may not necessarily remain constant as it is assumed in our analysis at temperatures near T_C and could be expected to be reduced (or entirely neutralized) via thermally excited carriers. Such a process may thus reduce (or completely eliminate) the built-in fields at temperatures near the T_C of strained PZT 30/70.

In Fig. 4, we provide the temperature dependence of the total polarization and the dielectric response for the case of a random space charge variation throughout the film thickness. Such a distribution introduces almost a linearly varying built-in field that changes sign near the middle of the film. This field results in a drastic reduction in T_C while there is a sharper dielectric anomaly at T_C compared to the conditions corresponding to asymmetric distribution of space charges discussed in connection with Fig. 3. We also note that the dielectric constant of the film with random variation in high density space charges at RT given in Fig. 4 is higher than the

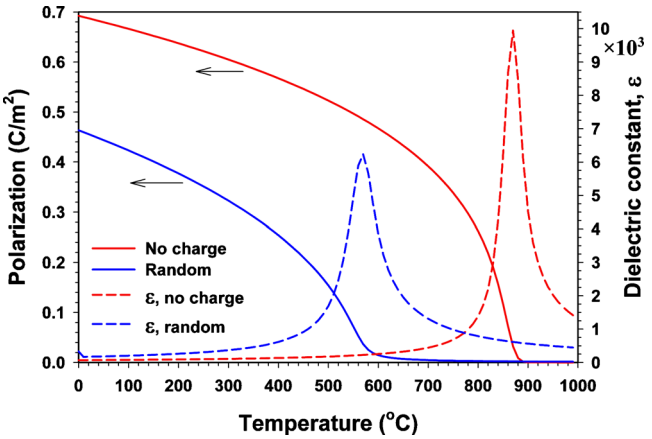

FIG. 4. (Color online) Total polarization and the dielectric constant as a function of temperature in the absence of space charges and with randomly distributed space charges with a maximum planar density of 0.05 C/m^2.

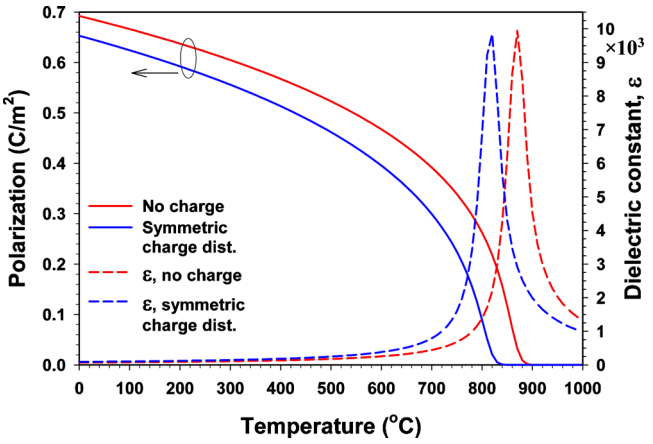

FIG. 5. (Color online) Total polarization and the dielectric constant as a function of temperature in the absence of space charges and with a completely symmetrical continuous distribution of space charge at both interfaces decaying exponentially toward the interior of the film.

films with $\rho=0$ because of the significant reduction in T_C, in agreement with the findings of Ref. 3. Above the effective T_C, there is nearly no net built-in polarization due to the opposite but nearly equal polarization profile in the two halves of the film with respect to the middle of the film at zero field.

Figure 5 plots the temperature dependence of the total polarization and the dielectric response in the case of a symmetrical charge distribution given in Fig. 1(c). A symmetrical variation in the planar space charge concentration removes any net internal bias in the system and the dielectric anomaly at T_C is nearly the same as that of the perfect film with no net built-in polarization except a slight reduction in T_C and P. From Fig. 5, one can observe a near zero built-in polarization above T_C as a consequence of the nearly equal internal field due to space charges in the two halves of the film. Due to the absence of a net bias field, the induced polarization due to space charges is weak and there is no smearing of the dielectric response at T_C. The fields due to space charges are mostly confined to the near-interface regions with exactly equal but opposite signs, giving rise to a symmetrical polarization variation below T_C. It should also be expected that the depolarizing field term has a more pronounced effect near the interfaces where the polarization changes drastically over relatively short distances. Thus, the small reduction in the remnant polarization at all temperatures below T_C compared to the charge-free film is mostly due to the inhomogeneous variation in the local polarization near the film-electrode interfaces. The changes in the polarization near the electrode interfaces also increases the gradient energy. Therefore, the combination of both the depolarization and the gradient energy act to slightly reduce T_C.

Overall, the gradual nature of the transition in the presence of asymmetric space charge dramatically reduces the dielectric anomaly that is a characteristic of the charge-free film in addition to a considerable drop in T_C. One must note that polarization, if computed for the FE phase with high space charge densities, is actually the susceptibility of the "pinned" or imprinted polarization concurrent with an asymmetrically distributed space charge. For thinner films, the same charge density distribution whose potential will become steeper (for zero potential at the electrodes), creating larger internal built-in fields can be expected to render a stronger P pinning highly probable. The strongly inhomogeneous fields acting at distances at the order of a few nanometers due to space charge lead to greater spatial variation in the polarization and hence yield higher depolarizing fields, resulting in a larger reduction in T_C, similar to the finite size effect.[35] This decrease should certainly be much more dramatic for highly asymmetrical distributions of space charges. We note that even if the switchable FE polarization disappears at temperatures above T_C, the space charge induced temperature-independent polarization will remain. In addition, a stronger smearing of the transition temperature could also be expected as already discussed in Ref. 36. This is, of course, possible for materials with low T_C wherein thermally excited neutralization mechanisms of space charges will not be significant. For films with high T_C, thermally excited carriers from the traps could take effect in neutralization of the space charges at elevated temperatures, reducing the smearing effects.

IV. CONCLUSIONS

Using a nonlinear thermodynamic model coupled with an electrostatic analysis, we have investigated the effects of a continuous distribution of planar space charges along the film thickness on the phase transition characteristics, hysteresis response, and dielectric properties of epitaxial (001) PZT 30/70 films between metallic electrodes on (001) STO substrates. It is shown that asymmetrically distributed space charges result in displacements in the $P-E_{APP}$ hysteresis curves along the applied field axis and may even give rise to coercive fields $E_{C-},E_{C+}>0$ or $E_{C-},E_{C+}<0$ compared to charge-free films for which $|E_{C-}|=E_{C+}$ and $\Delta E=E_{C+}-|E_{C-}|=0$. These trapped charges may significantly smear out the FE phase transition and reduce T_C. If the space charges are symmetrically distributed, the FE hysteresis loops shrink along both the polarization and the applied field axes but remain centered at the origin. For relatively high charge densities, we find that a monodomain FE film cannot be switched from one polarization state to another under typical cyclic (e.g., completely reversed sinusoidal) electrical bias with an amplitude $2\cdot E_{APP}$. A polydomain structure may form in FE films to minimize internal depolarizing fields originating from local variations in the polarization. However, the strong internal bias due to an asymmetric charge distribution may preclude the generation of electrical domains. The analysis presented herein is in the limit of thermodynamics and future time-dependent studies should focus on nucleation and growth kinetics of domains during switching in the presence of a spatial space charge distribution. In such dynamic models, the trapping and emission rates of carriers have to be considered as well.

ACKNOWLEDGMENTS

I. B. M. acknowledges the hardware and software support of Sabanci University. The work at the University of Connecticut was funded by the U.S. Army Research Office

through Grant Nos. W911NF-05-1-0528 and W911NF-08-C-0124.

[1]S. Triebwasser, Phys. Rev. **118**, 100 (1960).
[2]A. P. Levanyuk and A. S. Sigov, in *Defects and Structural Phase Transitions*, Ferroelectricity and Related Phenomena, edited by W. Taylor, Vol. 6 (OPA, Amsterdam, 1988).
[3]A. M. Bratkovsky and A. P. Levanyuk, Phys. Rev. B **61**, 15042 (2000).
[4]T. Pintilie and M. Alexe, J. Appl. Phys. **98**, 124103 (2005).
[5]Y. Xiao, V. B. Shenoy, and K. Bhattacharya, Phys. Rev. Lett. **95**, 247603 (2005).
[6]A. K. Tagantsev and G. Gerra, J. Appl. Phys. **100**, 051607 (2006).
[7]L. Pintilie, Phys. Rev. B **75**, 224113 (2007).
[8]L. Pintilie, I. Vrejoiu, M. Alexe, and D. Hesse, J. Appl. Phys. **104**, 114101 (2008).
[9]E. G. Lee, D. J. Wouters, G. Willems, and H. E. Maes, Appl. Phys. Lett. **69**, 1223 (1996).
[10]G. Le Rhun, R. Bouregba, and G. Poullain, J. Appl. Phys. **96**, 5712 (2004).
[11]See, for example, D. Balzar, P. A. Ramakrishnan, and A. M. Hermann, Phys. Rev. B **70**, 092103 (2004); I. B. Misirlioglu, S. P. Alpay, M. Aindow, and V. Nagarajan, Appl. Phys. Lett. **88**, 102906 (2006).
[12]M. Alexe, Appl. Phys. Lett. **72**, 2283 (1998).
[13]D. O'Neill, R. M. Bowman, and J. M. Gregg, Appl. Phys. Lett. **77**, 1520 (2000).
[14]J. Mcaneney, L. J. Sinnamon, A. Lookman, R. M. Bowman, and J. M. Gregg, Integr. Ferroelectr. **60**, 79 (2004).
[15]D. Fu, K. Suzuki, K. Kato, and H. Suzuki, Appl. Phys. A: Mater. Sci. Process. **80**, 1067 (2005).
[16]P. Zubko, D. J. Jung, and J. F. Scott, J. Appl. Phys. **100**, 114112 (2006).
[17]M. B. Okatan, J. V. Mantese, and S. P. Alpay, Phys. Rev. B **79**, 174113 (2009); Acta Mater. **58**, 39 (2010).
[18]L. Courtade, C. Muller, G. Andreoli, C. Turquat, L. Goux, and D. J. Wouters, Appl. Phys. Lett. **89**, 113501 (2006).
[19]L. Goux, Z. Xu, V. Paraschiv, J. G. Lisoni, D. Maes, L. Haspeslagh, G. Groeseneken, and D. J. Wouters, Solid-State Electron. **50**, 1227 (2006).
[20]W. B. Wu, K. H. Wong, C. L. Mak, C. L. Choy, and Y. H. Zhang, J. Vac. Sci. Technol. A **18**, 2412 (2000).
[21]W. B. Wu, K. H. Wong, and C. L. Choy, Appl. Phys. Lett. **85**, 5013 (2004).
[22]A. Z. Simoes, C. S. Riccardi, A. H. M. Gonzalez, A. Ries, E. Longo, and J. A. Varela, Mater. Res. Bull. **42**, 967 (2007).
[23]L. Feigl, E. Pippel, L. Pintilie, M. Alexe, and D. Hesse, J. Appl. Phys. **105**, 126103 (2009).
[24]A. K. Tagantsev, I. Stolichnov, N. Setter, and J. S. Cross, J. Appl. Phys. **96**, 6616 (2004).
[25]A. N. Morozovska and E. A. Eliseev, J. Phys. Condens. Matter **16**, 8937 (2004).
[26]Y. Zhou, H. K. Chan, C. H. Lam, and F. G. Shin, J. Appl. Phys. **98**, 024111 (2005).
[27]H. X. Cao, V. C. Lo, and Z. Y. Li, Solid State Commun. **138**, 404 (2006).
[28]I. B. Misirlioglu, M. Alexe, L. Pintilie, and D. Hesse, Appl. Phys. Lett. **91**, 022911 (2007).
[29]O. Dahl, J. K. Grepstad, and T. Tybell, J. Appl. Phys. **106**, 084104 (2009).
[30]X. J. Zheng, W. Yin, T. Zhang, Q. Chen, M. H. Tang, and J. Sun Phys. Status Solidi (RRL) **3**, 251 (2009).
[31]M. B. Okatan and S. P. Alpay, Appl. Phys. Lett. **95**, 092902 (2009).
[32]A. K. Tagantsev, Ferroelectrics **375**, 19 (2008).
[33]M. J. Haun, Z. Q. Zhuang, E. Furman, S. J. Jang, and L. E. Cross, Ferroelectrics **99**, 45 (1989).
[34]N. A. Pertsev, A. G. Zembilgotov, and A. K. Tagantsev, Phys. Rev. Lett. **80**, 1988 (1998).
[35]See, for example, E. K. Akdogan and A. Safari, J. Appl. Phys. **101**, 064114 (2007); **101**, 064115 (2007).
[36]A. M. Bratkovsky and A. P. Levanyuk, Phys. Rev. Lett. **94**, 107601 (2005).